40 Hz, with the responses falling off rapidly below 20 Hz, and more gradually above 50 Hz. A mean tuning curve for 13 primary afferents is shown in Fig. 2A.

Examinations of gut contents (*8, 9*) indicated that *P. borchgrevinki* feeds selectively on larger zooplankton in the upper water column. Recordings were made of vibrations produced during swimming by three crustacean species found in the diet of *P. borchgrevinki: Orchomene plebs* (Amphipoda), *Euphausia crystallorophias* (Euphausiacea), and *Euchaeta antarctica* (Calanoida). Swimming records (made by attaching the animals to a force transducer) were processed by a spectrum analyzer. They exhibited distinct low-frequency peaks at 3 to 6 Hz attributable to the basic rate of power strokes, several harmonics of the base frequency, and strong peaks between 30 and 40 Hz (Fig. 2B). The basic cycle of power and recovery stroke and the higher frequency components of the signal are evident in the swimming vibration record shown in Fig. 1. Nonswimming controls produced low-amplitude, low-frequency power spectra attributable to ventilatory movements, with a peak near 50 Hz due to electrical generator noise (*10*).

The correspondence between the frequency response characteristics of the anterior lateral line afferents and the power spectra of the swimming movements of their prey establishes the suitability of the anterior lateral line system for prey detection in *P. borchgrevinki.* We obtained direct confirmation of this relation by suspending an amphipod near the head of a fish while recording the activity of neurons from lateral line afferents (Fig. 1). Simultaneous strain gauge and nerve recordings showed bursts of nerve spikes with each cycle of power stroke and recovery, indicating that vibration produced by the swimming crustacean is a potent natural stimulus of the anterior lateral line system of the antarctic fish, which may be important in the close-range coordination of feeding.

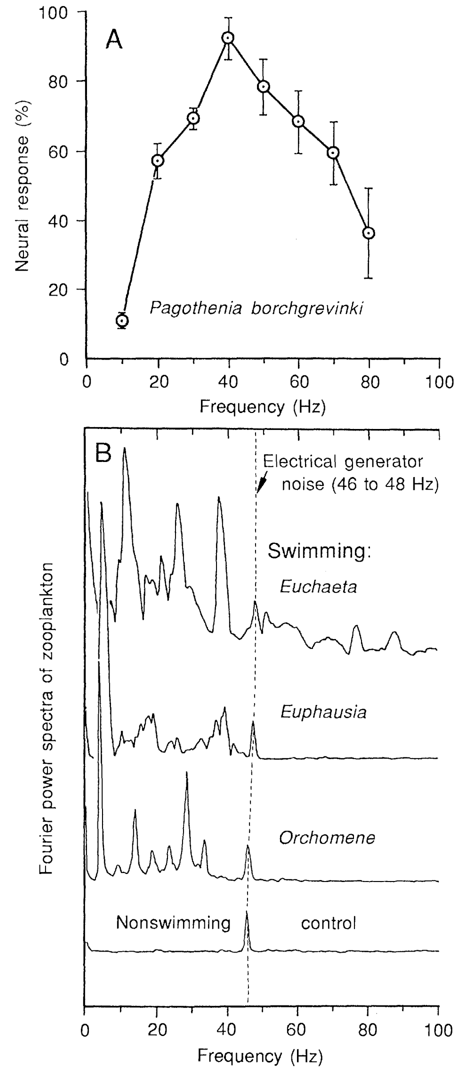

Fig. 2. (**A**) Frequency response characteristics of lateral line afferent fibers. Mean relative responses have been calculated for each vibration frequency for 13 fibers. Error bars indicate standard deviation. (**B**) Power spectra of strain gauge output attached to a swimming zooplankter (plotted with a linear vertical scale). Each spectrum was derived from swimming records consisting of 5 to 30 power stroke cycles.

REFERENCES AND NOTES

1. O. Sand, in *Hearing and Sound Communication in Fishes*, W. N. Tavolga, A. N. Popper, R. R. Fay, Eds. (Springer-Verlag, Berlin, 1981), pp. 459–480.
2. B. L. Partridge and T. J. Pitcher, *J. Comp. Physiol.* **135**, 315 (1980).
3. C. von Campenhausen, I. Riess, R. Weissert, *ibid.* **143**, 369 (1981).
4. T. Teyke, *ibid.* **157**, 837 (1985).
5. H. Bleckmann, *ibid.* **140**, 163 (1980).
6. J. C. Montgomery and A. J. Saunders, *Proc. R. Soc. London* **224**, 197 (1985).
7. A. J. Saunders and J. C. Montgomery, *ibid.*, p. 209.
8. J. T. Eastman and A. L. DeVries, *Polar Biol.* **4**, 45 (1985).
9. J. M. Cargill and J. C. Montgomery, *N.Z. Antarct. Rec.*, 7 (No. 1), 17 (1986).
10. Force transducer records included electrical noise from the portable generator used to power the recording apparatus. Loading of the generator caused it to run slightly slower than its rated frequency of 50 Hz.

11. We are grateful to B. A. Foster, J. D. Cargill, and G. D. Housley for assistance and advice during the experimental phase of this work. Supported by research grants from the New Zealand University Grants Committee and the Auckland University Research Committee. Logistic support was provided by the Antarctic Division of the New Zealand Department of Scientific and Industrial Research and the staff of Scott Base.

2 July 1986; accepted 16 October 1986

Disruption of the Mauna Loa Magma System by the 1868 Hawaiian Earthquake: Geochemical Evidence

ROBERT I. TILLING, J. MICHAEL RHODES, JOEL W. SPARKS,
JOHN P. LOCKWOOD, PETER W. LIPMAN

To test whether a catastrophic earthquake could affect an active magma system, mean abundances (adjusted for "olivine control") of titanium, potassium, phosphorus, strontium, zirconium, and niobium of historic lavas erupted from Mauna Loa Volcano, Hawaii, after 1868 were analyzed and were found to decrease sharply relative to lavas erupted before 1868. This abrupt change in lava chemistry, accompanied by a halved lava-production rate for Mauna Loa after 1877, is interpreted to reflect the disruptive effects of a magnitude 7.5 earthquake in 1868. This interpretation represents a documentable case of changes in magmatic chemical variations initiated or accelerated by a major tectonic event.

IGNEOUS PETROLOGISTS TYPICALLY ANalyze and interpret chemical variations of volcanic rocks in terms of physicochemical processes intrinsic to a given magmatic system. Most investigators assume, implicitly or explicitly, that processes producing chemical changes operate gradually during the lifetime of that system. We present evidence that a catastrophic event, the great 1868 earthquake, may have disrupted the magma system at Mauna Loa Volcano, Hawaii, and affected the chemistry of its lavas for decades thereafter.

Mauna Loa (Fig. 1), the world's largest active basaltic volcano, last erupted in March and April 1984 (*1*). Earlier petrologic studies of Mauna Loa tholeiitic basalt (*2, 3*) showed that nearly all of the major-element variation can be accounted for by the addition or subtraction of olivine [called "olivine control" by Powers (*2*)]. A few volumetrically small tholeiites are more evolved as a result of differentiation involving pyroxene and plagioclase in addition to olivine (*3, 4*). A study of 114 samples of historic Mauna

---

R. I. Tilling, U.S. Geological Survey, National Center, Reston, VA 22092.
J. M. Rhodes and J. W. Sparks, University of Massachusetts, Amherst, MA 01003.
J. P. Lockwood, U.S. Geological Survey, Hawaiian Volcano Observatory, HI 96718.
P. W. Lipman, U.S. Geological Survey, Denver, CO 80225.

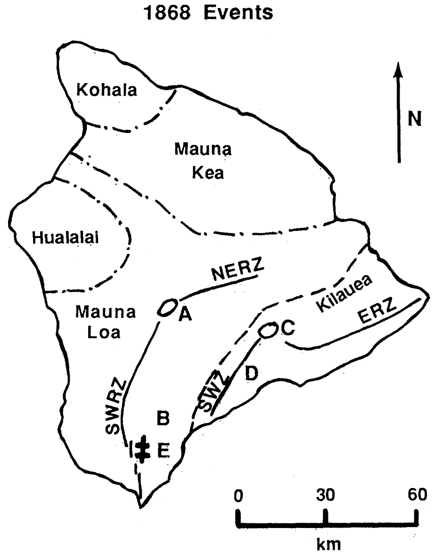

Fig. 1. Map showing the five volcanoes making up the Island of Hawaii, the inferred epicenter of the great 1868 earthquake, and the sites of eruptive activity at Mauna Loa and Kilauea from 27 March to 11 April 1868. Mauna Loa: SWRZ, southwest rift zone; NERZ, northeast rift zone; A, summit eruption of 27 March; B, earthquake (magnitude 7.5), 2 April; E, southwest rift eruption of 7 to 11 April. Kilauea: SWZ, southwest rift zone; ERZ, east rift zone; C, Kilauea Iki eruption of 2 April; D, southwest rift eruption of 2 April.

Loa lava showed that most flow fields are remarkably homogeneous despite differences in volume, duration of eruption, or vent site (*5*).

By adjustment of lava chemistry to a constant MgO content to remove the effect of olivine control, Wright (*3*) recognized significant major-element differences between time-grouped Kilauea lavas (prehistoric, 18th and 19th century, and 20th century), but found no differences among similarly grouped Mauna Loa lavas. The validity of the MgO-adjustment procedure (*6*) appears to be well demonstrated (Fig. 2) by two 1868 lava samples, a "normal" tholeiite (W-A-7) and an olivine-rich picrite (1868ML), which span the greatest range in MgO content (raw data) of any of the Mauna Loa flows. Some later investigators, although recognizing small but significant temporal variations in MgO-adjusted incompatible-element abundances, emphasized the lack of major changes in MgO-adjusted compositional characteristics throughout more than 31,000 years of Mauna Loa's eruptive history (*7*). These episodic fluctuations in lava composition have been interpreted to result from diverse magma-mixing processes or a highly heterogeneous mantle source (or both) rather than from partial melting or magma differentiation mechanisms (*8, 9*).

Some recent studies (*10, 11*), however, suggest that variations in chemical composition of Mauna Loa lava may also define a subtle but systematic temporal trend: MgO-adjusted mean abundances of the olivine-incompatible elements tend to decrease with time. Although some of the observed differences in mean composition of the time-grouped Mauna Loa lavas are within analytical uncertainty (Table 1), these minor differences are nonrandom and cannot be ascribed to possible bias introduced by laboratory procedures (*10, 11*).

Although the statistical validity of the apparent long-term variation trend for Mauna Loa lava needs to be tested with larger sample populations, the existence of a sharp compositional break between the lavas of 1868 and 1880 is clear (Figs. 3 and 4). This "sudden drop between 1868 and 1880" was earlier considered as part of the "episodic variation" for Mauna Loa lavas (*7*). We interpret this compositional break as reflecting the possible disruption of the Mauna Loa magma system by the great 1868 earthquake (*12*); such a possible disruption is independently suggested by Lockwood and Lipman (*13*) on the basis of an abrupt decrease in lava-production rate after 1877.

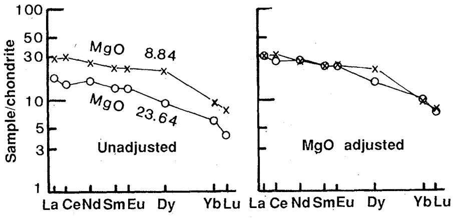

Fig. 2. Chondrite-normalized abundances of rare-earth elements in two samples of lava formed during a 5-day eruption of Mauna Loa in 1868, illustrating their close similarity after adjustment (MgO = 7.00% by weight) (*11*). Sample W-A-7 (X) is a normal tholeiite (8.84% MgO by weight) erupted early and sample 1868ML (O) is a picrite (23.64% MgO by weight) produced later in the same eruption.

Our interpretation is predicated on the compositional variations with time shown in Figs. 3 and 4. The data of Rhodes (*5*), which represent the MgO-adjusted mean values of 3 to 12 samples for each eruption, exhibit striking parallelism in variations of the olivine-incompatible elements, even for small changes (for example, between the 1949 and 1950 eruptions). Values of elements for eruptions before and after the 1868 earthquake show little or no overlap. In addition to the variation patterns defined by the trace elements strontium, zirconium, and niobium (Fig. 3), two sets of available data for the elements titanium, potassium, and phosphorus show similar patterns (Fig. 4). A slight interlaboratory bias exists, but the overall agreement is excellent even though the analyses were done years apart in different laboratories, with different sample powders and analytical techniques. The more extensive data of Rhodes (*5*) better express the abrupt step decrease than those of Wright (*3*), which mostly consist of a single analysis for each flow. We interpret the plotted curves (Figs. 3 and 4) to show: (i) an abrupt step decrease in the MgO-adjusted mean abundances of Ti, K, P, Sr, Zr, and Nb following the 1868 earthquake; and (ii) the decades-long recovery of the Mauna Loa magmatic system from the disruptive effects of the earthquake, as expressed by gradually increasing abundances of these elements to approach pre-earthquake levels. However, other evidence (*9*) suggests that the observed compositional shift after 1868 may primarily represent only the acceleration of an already established trend of decreasing olivine-incompatible elements, rather than a step decrease.

The 1868 earthquake, centered along the southeast flank of Mauna Loa (Fig. 1), was the largest to strike the Island of Hawaii in recorded history. Estimated to have a Richter magnitude of about 7.5 (*14*), the 1868 earthquake and associated tsunami caused great destruction throughout the southern part of the island. It occurred on 2 April 1868, shortly after a 1-day summit eruption of Mauna Loa on 27 March. On the same day, the 1868 earthquake apparently also triggered two small eruptions in different

Table 1. MgO-adjusted mean abundances (±SD) of selected olivine-incompatible elements in Mauna Loa lavas grouped according to time (*11*, table 24.20).

Oxide or element	Abundance		
	Prehistoric ($n = 10$)	19th century ($n = 8$)	20th century ($n = 6$)
		Percent by weight	
K_2O	0.44 ± 0.03	0.40 ± 0.05	0.37 ± 0.02
TiO_2	2.16 ± 0.11	2.11 ± 0.13	2.08 ± 0.03
P_2O_5	0.24 ± 0.02	0.23 ± 0.02	0.21 ± 0.01
		Parts per million	
La	10.2 ± 1.5	9.4 ± 1.0	8.7 ± 0.4
Ce	25.8 ± 4.7	24.6 ± 2.3	21.8 ± 2.2
Nd	17.6 ± 2.2	17.1 ± 1.4	16.7 ± 0.5
Sm	4.68 ± 0.48	4.66 ± 0.19	4.45 ± 0.26

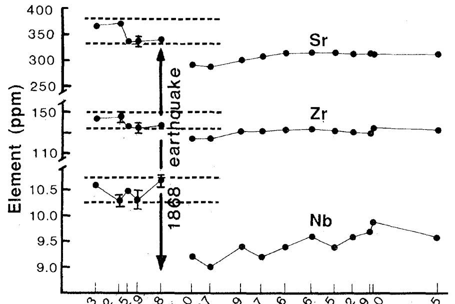

Fig. 3. The MgO-adjusted mean abundances of the olivine-incompatible trace elements Sr, Zr, and Nb in the historic Mauna Loa lavas. The plotted points are calculated from average compositions given by Rhodes (*5*) (114 analyses total); unless stated otherwise, a 1-SD error falls within the plotted points. The discontinuity shown between the eruptions of 1868 and 1880 is interpreted to be an effect of the 1868 earthquake.

parts of neighboring Kilauea Volcano (Fig. 1) and a 100-m subsidence of the floor of Kilauea caldera.

On 7 April, eruption began in the southwest rift zone of Mauna Loa, marking the first historic activity in that sector of the volcano. The first lava erupted was characterized by moderate MgO content [~9% MgO by weight, according to Rhodes (*5*)]; later, lavas were distinctly picritic (~20% MgO by weight), containing abundant olivine phenocrysts. The eruptive fissure was localized at the lowest elevation (600 to 900 m) of any historic vent, in a segment of the southwest rift in which no major eruption had occurred for thousands of years. Apparently the 1868 earthquake opened up a lower part of the rift zone and reestablished magmatic communication with Mauna Loa's summit that had been blocked a long time (*15*).

The eruptive activity, which ended on 11 April 1868, is interpreted to have successively tapped the upper part (with normal olivine content) and then the lower part (olivine-rich) of a magma reservoir that was zoned as a result of olivine settling (*15*). Mauna Loa's magma reservoir may have been substantially drained by the 1868 eruption and earthquake, as suggested by major collapse of the summit caldera during or shortly after 1868 (*13*). Such an interpretation is compatible with the fact that the average lava-production rate for Mauna Loa after 1877 is less than half that before 1877 (Fig. 5). The relatively small erupted volume (subaerial and below-sea nearshore) of the 1868 activity, only about 130 × 10^6 m^3 (*13*), implies that the magma stored in the reservoir before 1868 drained by leakage into subsurface parts of the southwest rift zone or possibly by undetectable eruption in the deep submarine extension of the rift zone, or both.

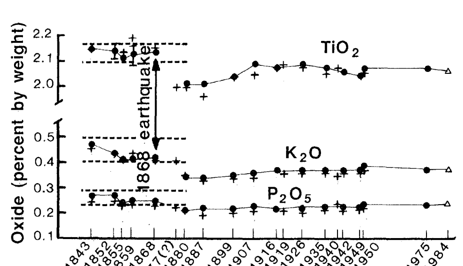

Fig. 4. The MgO-adjusted mean abundances of the olivine-incompatible elements Ti, K, and P (expressed as oxides) in the historic Mauna Loa lavas, calculated from the data of Rhodes (*5*) (●), Wright (*3*) (+), and Lockwood *et al.* (*1*) (△). Unless stated otherwise, the 1-SD error falls within plotted points. The variation patterns, including the presumed earthquake-induced discontinuity, mimic those in Fig. 3.

We propose the following scenario to account for our observations. (i) The 1868 earthquake disrupted the magma system at Mauna Loa, permitting the tapping of the lower (olivine-rich) part of the shallow zoned magma reservoir during the 1868 eruption. The summit reservoir and supplying conduit system was largely emptied during or shortly after the activity, presumably by massive leakage into the earthquake-shattered southwest rift zone, because the volume of lava erupted is far too small to drain the reservoir. (ii) The lavas erupted during the two decades following the 1868 earthquake were the most depleted in incompatible elements, suggesting derivation from magmas that had recently arrived from the mantle-source region and had spent little or no time in the intermediate-level reservoirs to permit mixing or fractionation before storage in, and eruption from, the shallow reservoir. (iii) The 1899 and later eruptions successively produced lavas somewhat more enriched in incompatible elements, suggesting a gradual, decades-long recovery of the disrupted Mauna Loa magma supply system from the 1868 earthquake, as "normal" communication was reestablished between the magma-source regions and shallower storage zones. If the postulated long-term trend of decreasing incompatible elements with time for Mauna Loa lava (*10, 11*) is confirmed, this recovery process can be taken to indicate a reapproach to the long-term trend following a short-term perturbation caused by the 1868 earthquake.

The data on lava chemistry suggest that Mauna Loa's magma system is recovering from the 1868 earthquake, but the data for lava-production rate since 1877 do not. This apparent noncorrespondence is not understood, but we offer two explanations, both speculative. First, while the balance between

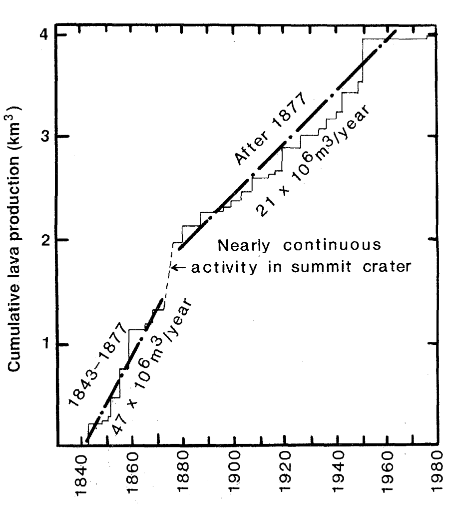

Fig. 5. Lava-production rate for Mauna Loa Volcano decreases by more than a factor after 1877 [modified from Lockwood and Lipman (*13*, figure 7)]. The change in lava-production rate is interpreted as another effect of the 1868 earthquake.

magma supply and magma storage has been largely restored, the part of the system linking the shallow reservoir and the surface remains out of balance. Alternatively, the intermediate and higher parts of the system have reestablished balance, but the supply rate of magma from the mantle-source region decreased after 1877. The latter proposal is compatible with the "hot spot" hypothesis for Hawaiian volcanism (*16*), according to which Mauna Loa's lava production should diminish with time and ultimately cease as continued, relative, northwestward movement of the Pacific Plate progressively carries the volcano away from its magma source over the fixed hot spot.

Our results provide a documented case of a violent tectonic event upsetting the delicate balance of Mauna Loa's magma system, as reflected in its lava chemistry and lava-production rate for decades afterward. Changes in magma chemistry need not be gradual and could be initiated or accelerated by a catastrophic event external to the magmatic system. Such phenomena should not be restricted to Mauna Loa Volcano, even though for other magma systems the task of recognizing earthquake-induced variations in the composition of igneous suites may be formidable. Dynamic changes in the magma regime of neighboring Kilauea Volcano have been attributed to the magnitude 7.2 Kalapana earthquake in 1975 (*17*) and to the magnitude 6.2 Honomu earthquake in 1973 (*18*). Whether or not the effect of these earthquakes is also evident in Kilauea lava has not been evaluated.

REFERENCES AND NOTES

1. J. P. Lockwood *et al.*, *Eos* 66, 169 (1985).
2. H. A. Powers, *Geochim. Cosmochim. Acta* 7, 77 (1955).

3. T. L. Wright, *U.S. Geol. Surv. Prof. Pap. 735* (1971).
4. J. M. Rhodes *et al.*, *Eos* **64**, 900 (1983); J. W. Sparks and J. M. Rhodes, *Geol. Soc. Am. Abstr. Program* **15**, 692 (1983).
5. J. M. Rhodes, *J. Geophys. Res.* **88** (suppl.), A869 (1983).
6. The procedure to adjust analyses to MgO = 7.00 (percent by weight) involves the subtraction or addition of olivine of Fo$_{87.5}$ composition [that is, containing 87.5% of the magnesian end-member (forsterite) in solid solution], the same average composition as used by Wright (*3*), and is described elsewhere (*11*, appendix).
7. J. M. Rhodes and P. W. Lipman, *Abstracts, Hawaii Symposium on Intraplate Volcanism and Submarine Volcanism* (International Association of Volcanology and Chemistry of Earth's Interior, Hilo, HI, 1979), p. 97; J. M. Rhodes, J. P. Lockwood, P. W. Lipman, *Abstracts, Generation of Major Basalt Types* (International Association of Volcanology and Chemistry of Earth's Interior–International Association of Geochemistry and Cosmochemistry, Reykjavik, Iceland, August 1982), abstr. 43.
8. J. M. Rhodes, *Eos* **64**, 348 (1983).
9. ______ and J. W. Sparks, *Proc. Inst. Stud. Earth Man Conf. Open Magmatic Systems* (August 1984), p. 135 (extended abstr.).
10. J. R. Budahn and R. A. Schmitt, *Geochim. Cosmochim. Acta* **49**, 67 (1985).
11. R. I. Tilling, T. L. Wright, H. T. Millard, Jr., *U.S. Geol. Surv. Prof. Pap.*, in press.
12. R. I. Tilling, *Eos* **66**, 851 (1985).
13. J. P. Lockwood and P. W. Lipman, *ibid.*, in press.
14. D. C. Cox and J. Morgan, *Univ. Hawaii, Hawaii Inst. Geophys. Rep. 77-14* (1977).
15. P. W. Lipman, *Bull. Volcanol.* **43**, 703 (1980).
16. G. B. Dalrymple, E. A. Silver, E. D. Jackson, *Am. Sci.* **47**, 45 (1973); D. A. Clague and G. B. Dalrymple, *U.S. Geol. Surv. Prof. Pap.*, in press.
17. D. Dzurisin and R. Y. Koyanagi, *U.S. Geol. Surv. Open-File Rep. 81-571* (1981); D. Dzurisin, R. Y. Koyanagi, T. T. English, *J. Volcanol. Geotherm. Res.* **21**, 177 (1984).
18. R. I. Tilling *et al.*, *U.S. Geol. Surv. Prof. Pap.*, in press.

19. We thank the staff members of the U.S. Geological Survey Hawaiian Volcano Observatory for support and cooperation in the sampling of the Mauna Loa eruptive products, and R. T. Helz and B. C. Hearn for constructive comments on the manuscript. Supported by NASA grant NSG-9060 and NSF grant EAR-84-18671 to J.M.R. and J.W.S.

16 June 1986; accepted 10 October 1986

Oxygen Supersaturation in the Ocean: Biological Versus Physical Contributions

H. CRAIG AND T. HAYWARD

A method based on measurements of dissolved molecular nitrogen, molecular oxygen, and argon can distinguish biological from physical contributions to oxygen supersaturation in the ocean. The derived values of biological O_2 production can be used as a check on estimates of total organic productivity measured by instantaneous rates of carbon-14 assimilation. Application to the shallow summer O_2 maxima in the North Pacific gyres shows that about 72% of the O_2 supersaturation maximum at 28°N and about 86% of the maximum at 40°N are due to net photosynthetic production.

THE MAGNITUDE OF PRIMARY PRODUCTION in the world oceans is controversial because of uncertainties in the methods of estimating productivity in the sea (*1, 2*). Central to this problem is the comparison of organic productivity, measured by means of instantaneous ^{14}C uptake, with seasonal data on accumulation rates of dissolved oxygen below the surface mixed layer, and central to that comparison is a knowledge of the relative proportions of physical and biological contributions to oxygen supersaturation. We discuss here the development of the subsurface dissolved molecular oxygen (O_2) maximum in the North Pacific gyre during summer. Reid (*3*) explained this maximum and its attendant O_2 supersaturation as a virtual effect caused by loss of O_2 from surface water by warming and gas exchange, leaving an induced O_2 maximum below. Shulenberger and Reid (*4*) later pointed out that these processes cannot account for the actual O_2 supersaturation and proposed that the major cause is photosynthetic production of O_2 below the base of the shallow mixed layer. They also concluded that productivity measured by ^{14}C uptake in these waters was much lower than values derived from O_2 production rates, thereby initiating a debate that has continued with vigor (*5–9*).

Table 1. N_2, O_2, and Ar saturation anomalies (Δ) for air injection and postequilibration potential temperature changes in seawater at 15°C and a salinity of 34 per mil. Row 3 gives the anomalies resulting from mixing equal parts of 10°C, 34.5 per mil and 20°C, 35 per mil seawater. Row 4 compares the products of Bunsen solubility coefficients and molecular diffusion coefficients for N_2 and O_2 in seawater at 22°C, to the same product for Ar (*10*). Solubility equations of Weiss (*11*) are used throughout.

Process	N_2	O_2	Ar
Air injection (1 ml/kg)	7.67%	3.75%	3.42%
ΔT = 1°C	1.79%	2.00%	2.01%
Mixing (10° + 20°)	0.86%	0.98%	0.94%
$(\beta D)_i/(\beta D)_{Ar}$ (22°C)	0.38	0.90	1

We describe here a technique for precise determination of biological and physical contributions to O_2 supersaturation that is based on the use of dissolved argon (Ar) as a biologically inert surrogate for oxygen. Our method parallels a previous similar development (*10*) for evaluating the contributions of air injection and hydrothermal input to oceanic helium concentrations based on the use of dissolved neon (Ne) and Ar. In the present work we use molecular nitrogen (N_2) and Ar saturation anomalies to derive the contributions of air injection and net photosynthetic production to the O_2 supersaturation.

As in (*10*), we write the saturation anomaly for a gas as $\Delta_i = (C_i/C^*_i) - 1$, where C_i is the observed concentration and C^*_i is the gas concentration at saturation equilibrium. The saturation anomaly is the sum of the effects of barometric pressure variations, temperature changes in the water parcel after atmospheric equilibration, air injection (by downward transport of bubbles), and, in the case of O_2, a contribution, Δ_J, from the net photosynthetic production of O_2:

$$\Delta_i(\%) = \Delta_P - 100\,(d\ln C^*_i/dT)\,\Delta T + (x^A_i/C^*_i)\,a + \Delta_J \tag{1}$$

where Δ_P is the percentage deviation of barometric pressure from 1 atm during equilibration, ΔT is the potential temperature change of the water parcel after equilibration, x^A_i is the volume fraction of the gas in dry air, and a is the amount of injected air in concentration units. Although, in principle, measurement of three conservative components, for example, N_2, Ar, and Ne, is necessary to define the pressure, temperature, and air injection contributions, the close similarity of Ar and O_2 solubility parameters allows precise evaluations of the air injection and Δ_J terms for O_2 to be made from measurements on N_2 and Ar. Table 1 compares the effects of air injection and temperature changes on N_2, O_2, and Ar saturation anomalies, together with the supersaturation in mixing due to the nonlinearity of C^* versus T. The effects of O_2 and Ar are essentially indistinguishable for these processes. Also shown are the relative $\beta_i D_i$ products (defined in Table 1) that govern the equilibration kinetics between bubbles and solution for the various gases (*10*) and that are also similar for O_2 and Ar. The primary difference is the air injection coefficient for N_2 compared with that of Ar, which can be used to evaluate the injected air component from Eq. 1 for these two gases:

$$a = 0.235\,(\Delta N_2 - \Delta Ar) + 0.053\,\Delta T \tag{2}$$

Scripps Institution of Oceanography, University of California, San Diego, La Jolla, CA 92093.